UNIVERSITA' DEGLI STUDI DI PADOVA

DIPARTIMENTO DI SCIENZE CHIMICHE

CORSO DI LAUREA IN CHIMICA INDUSTRIALE

TITOLO DELLA TESI

SYNTHESIS AND CHARACTERIZATION OF NOVEL CHLORO-SUBSTITUTED TRIS(PYRIDYLMETHYLAMINE) COBALT COMPLEXES FOR APPLICATIONS IN REDUCTION CATALYSIS

Relatore: Prof. Cristiano Zonta

Laureanda: Elisa Savastano
1226200

Anno Accademico 2021/2022

TABLE OF CONTENTS

1. INTRODUCTION 4

1.1 Ligands in coordination chemistry 4

1.2 Tris(2-pyridilmethyl)amine ligands (TPMA) 4

1.3 TPMA complexes and their applications 5

1.4 TPMA complexes in reduction catalysis 6

1.4.1 Hydrogen Evolution Reaction (HER) 6

1.4.2 Cobalt polypyridine complexes for HER 8

1.5 Carbon Dioxide Reduction 9

1.5.1 Cobalt TPMA complex for electrochemical reduction of CO_2 11

2. THE AIM OF THE THESIS WORK 14

3. RESULTS AND DISCUSSION 15

3.1 Synthesis of *para*-substituted tris(2-pyridilmehyl)amine 15

3.2 Chloro-substituted TPMA 16

3.3 Synthesis of Cobalt-TPMA complexes 17

3.4 Cyclic Voltammetry 18

4 CONCLUSIONS 20

5 EXPERIMENTAL PART 21

5.3 General methods 21

5.4 Abbreviations 21

5.5 Characterization of 1-(4-chloropyridin-2-yl)-N-((4-chloropyridin-2-yl) methyl-N-(pyridine-2-ylmethyl)methanamine 26 22

5.6 Characterization of Co-TPMA complexes 28-29 22

6 REFERENCES 25

1. INTRODUCTION

1.1 Ligands in coordination chemistry

In coordination chemistry, ligands are used to control the environment of metal centers modulating their electronic and steric properties. One of the main challenge for scientists is to design new molecular structures inspired by nature. In this context, synthetic transition metal complexes represent a large category of catalysts where ligands modulate the electronic and steric properties, and the metal governs the activity of the catalyst[1].

Beside the catalytic activity, metal complexes have also found several applications in supramolecular chemistry as building blocks for synthesis of supramolecular architectures due to their thermodynamic stability and the possibly to exploit also molecular recognition[2]. Among many different ligands, polypyridines are one of the widest groups of polydentate ligands reported in literature.

1.2 Tris(2-pyridylmethyl)amine ligands (TPMA)

A significant class of ligands is represented by tripodal ligands having three pyridyl systems linked to a central nitrogen atom (**Figure 1**). Among this class, the most common ligands are tris(2-pyridylmethyl)amine (**TPMA**), in which the position of nitrogen atoms on the aromatic rings allows the formation of four coordination bonds with a central ions. Steric and electronic characteristics of the tripodal ligand can be changed by modifying the substituents of the pyridyl units[3,4].

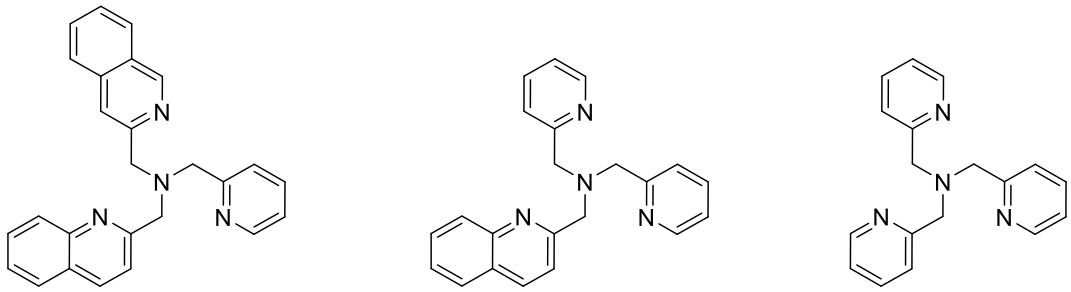

Figure 1: Structure of bis(2-quinolylmethyl)2-pyridylmethylamine **BQPA**, bis(2-pyridylmethyl)-2-quinolyamine **BPQA**, tris(2-pyridylmethyl)amine **TPMA** ligands.

The ligand was first obtained in 1967[5,6] by Andreg and Wank using alkylation of primary (2-pyridyl)methylamine **1** with two equivalents of (chloromethyl)pyridine **2** in NaOH aqueous solution (**Scheme 1**). A brown solid was obtained after recrystallization from water (90 % yield).

However, in recent years reductive amination has proved to represent a valuable alternative to alkylation. In this case, an aldehyde precursor **3** reacts with ammonium acetate as nitrogen source and sodium triacetoxyborohydride as reducing agent.

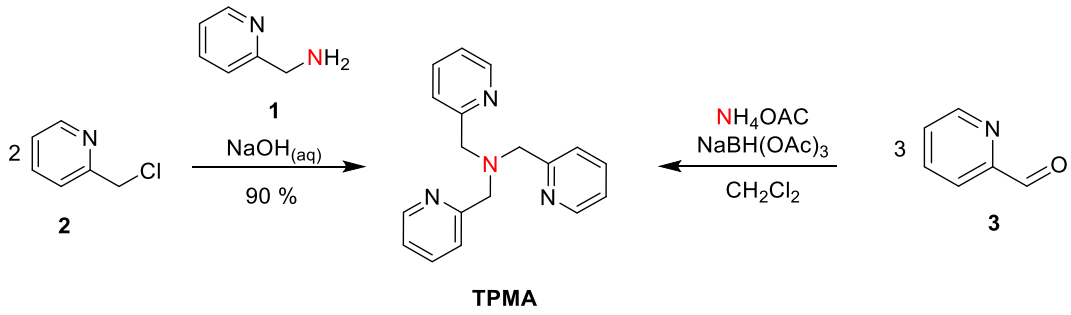

Scheme 1: Alkylation and reductive amination for **TPMA** synthesis

1.3 TPMA complexes and their applications

The first **TPMA** metal complex was reported in 1969 and had iron as central metal. This iron complex is still the most studied, although other metals such as cobalt, copper, zinc, nickel, ruthenium, and manganese have been reported through the years (**Figure 2**).

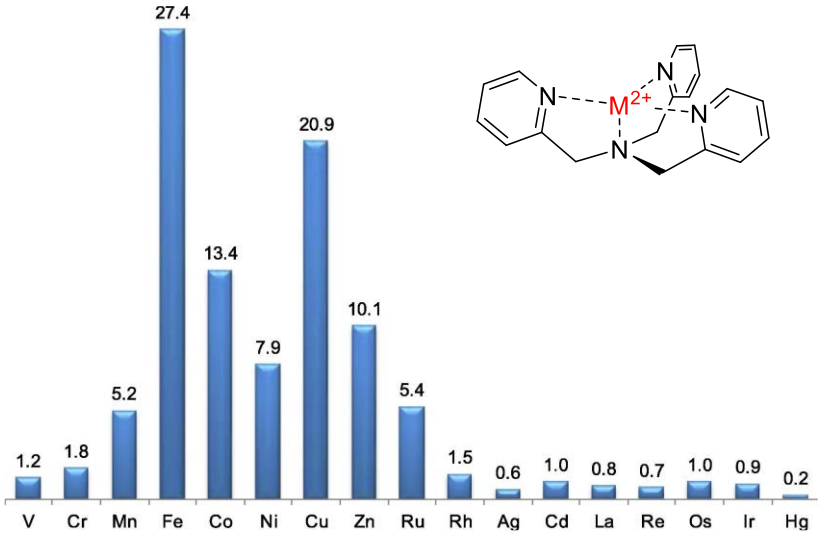

Figure 1: Metal distribution in crystallographic structures based on **TPMA** ligands. (Cambridge Crystallographic Data Centre, 2019).

The most common geometry of metal-based **TPMA** complex is trigonal bipyramidal,

where one apical position is occupied by the amine-type nitrogen and three equatorial positions are occupied by pyridine nitrogen atoms of **TPMA** ligand. The other apical position is usually occupied by a monodentate ligand or by a solvent molecule. Other geometries are less common, octahedral complexes are obtained preferentially with Iron or Nickel and tetrahedral coordination is scarcely observed because bite angle of the **TPMA** is not wide enough[7,8,9].

TPMA metal complexes have a wide range of catalytic applications from hydrogen production with cobalt, iron or nickel complexes[10,11], atom transfer radical addition and polymerization with copper complexes[12], carbon dioxide reduction with cobalt complexes[13.14]. In the group where this thesis has been carried out, **TPMA**-based systems have been extensively studied over the years and they have found applications in different areas such as the determination of enantiomeric excess of a wide range of substrates[15,16] and the reductive catalysis[10,11,13,14]. The work of this thesis is focused on the latter purpose which will be deepened in the next chapter.

1.4 TPMA complexes in reduction catalysis

1.4.1 Hydrogen Evolution Reaction (HER)

Using light to drive highly endothermic reactions transforming abundant and low energy raw materials into high added value molecules is the ambitious purpose of a significant part of the scientific community[17]. This is well-represented by the much-desired Hydrogen Evolution Reaction (HER):

$$2H^+ + 2e^- \longrightarrow H_2 \qquad (1)$$

Extracting electrons from water is though particularly difficult and requires several processes, which are at the very core of artificial photosynthesis research field.

The photosynthetic evolution of H_2 is performed using a particular artificial photosystem called “three-component system”[18]. Those three components are: 1) a photosensitizer ($Ru(bpy)_3^{2+}$, or generally PS), 2) a sacrificial electron donor (SD), which is ascorbate and 3) the cobalt polypyridine complex (**Figure 3**).

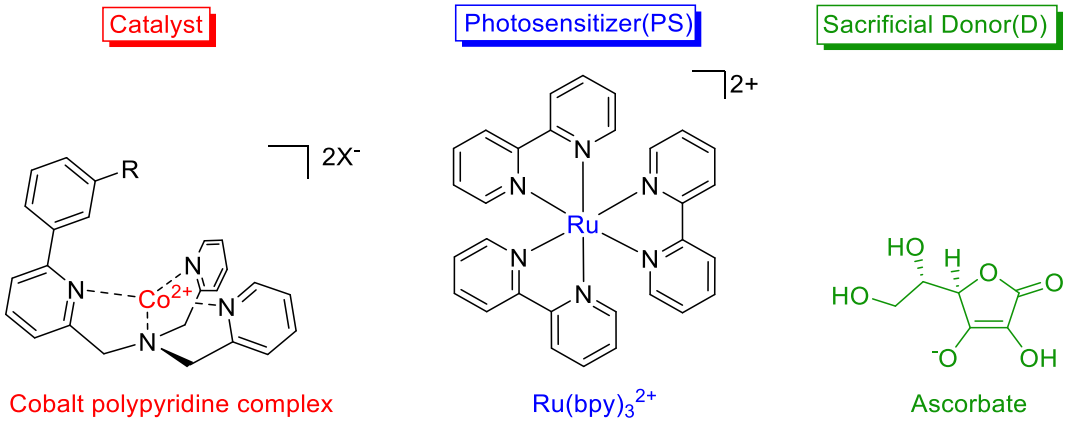

Figure 3: Standard photochemical system for HER involving a catalyst based on cobalt polypyridine complex, a photosensitizer based on $Ru(bpy)_3^{2+}$ and ascorbate as sacrificial donor.

Working with these three-component system, both oxidative and reductive quenching pathways can be used: for oxidative quenching, $Ru(bpy)_3^{2+}$ is supposed to be irradiated undergoing oxidative extinction by the catalyst that passes to a reduced form and an oxidized chromophore is obtained. Then is reduced again by reacting with the ascorbate (**Scheme 2**). In reductive quenching, $*Ru(bpy)_3^{2+}$ can abstract an electron from the ascorbate first, and then is regenerated by transferring an electron to the catalyst. The photoinduced electron transfer observed in the oxidative process between the excited state of the photosensitizer and the catalyst usually occurs with a bimolecular rate constant of 10^9 $M^{-1}s^{-1}$ [10,18], whereas the rate constant for reductive electron transfer involving the ascorbate donor is 10^7 M^{-2} s^{-1} in aqueous solution. Based on this kinetic data, pseudo first order rate constants can be estimated in the range 10^3-10^5 s^{-1} by the oxidative pathway of $*Ru(bpy)_3^{2+}$ by the cobalt complex, while values of $>10^6$ s^{-1} are estimated by the reductive pathway of $*Ru(bpy)_3^{2+}$ from ascorbate. The rate of the reductive process is ten times higher than the oxidative one and this establishes that the light-driven evolution of hydrogen using the three-component system follows a reductive quenching path.

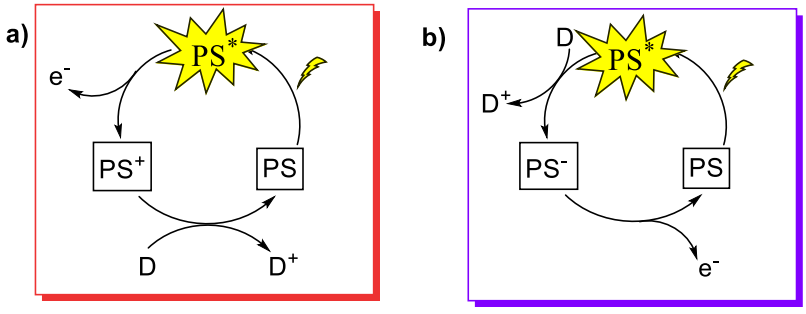

Scheme 2: Mechanisms of **a)** oxidative and **b)** reductive quenching to produce H_2 from water.

1.4.2 Cobalt polypyridine complexes for HER

In recent years, the use of cobalt complexes based on polypyridine ligands or amine-polypyridines ligands is increasing in reduction reactions such as Hydrogen Evolution Reaction (HER) under photochemical conditions (**Figure 4**). In 1981, Sutin *et al*. studied a cobalt-based polypyridine system which, working under photochemical conditions with $Ru(bpy)_3^{2+}$ as a photosensitizer and ascorbate as a sacrificial donor, catalysed the reduction of hydrogen to aqueous solution at pH = 5[20,21].

In 2010 Chang *et al*. presented a new cobalt octahedral complex based on a polypyridine ligand (**9**) which had two free coordination sites to be used in reduction reactions. The complex is able to reduce hydrogen protons under electrochemical condition with a Faraday yield of 99% in acetonitrile solution, or 50% aqueous solutions, in the presence of trifluoroacetic acid (TFA) which triggers the appearance of a catalytic wave close to the catalytic pair $Co^{(II)}/Co^{(I)}$ of **9**[22].

In 2014, Thummel *et al*. introduced a new cobalt catalyst based on a planar polypyridine ligand (**10**) with two axial chlorides ligands that catalysed light-driven hydrogen reduction in an aqueous environment. Under irradiation with blue light, at pH = 4 and utilizing $Ru(bpy)_3^{2+}$ and ascorbate as photosensitizer and sacrificial donor results in a TON = 333 and a TOF = 586 h^{-1} after 3 h[23].

In 2016 Blackman *et al*., studied the influence of the apical ligand in a polypyridine complex of cobalt (**13**) used for the photochemical reduction of hydrogen in water solution using the same multicomponent system showed in **Figure 3**. Among the various anionic ligands studied (X = Cl^-, NO_3^-, $CF_3SO_3^-$, H_2O) the complex showing the best catalytic activity is chlorine adduct (TON_{cat} = 13,5). In addition, by adding NaCl (0.3 M) the TON_{cat} increases by a factor of 2 for X = Cl^-, $CF_3SO_3^-$, and H_2O[24].

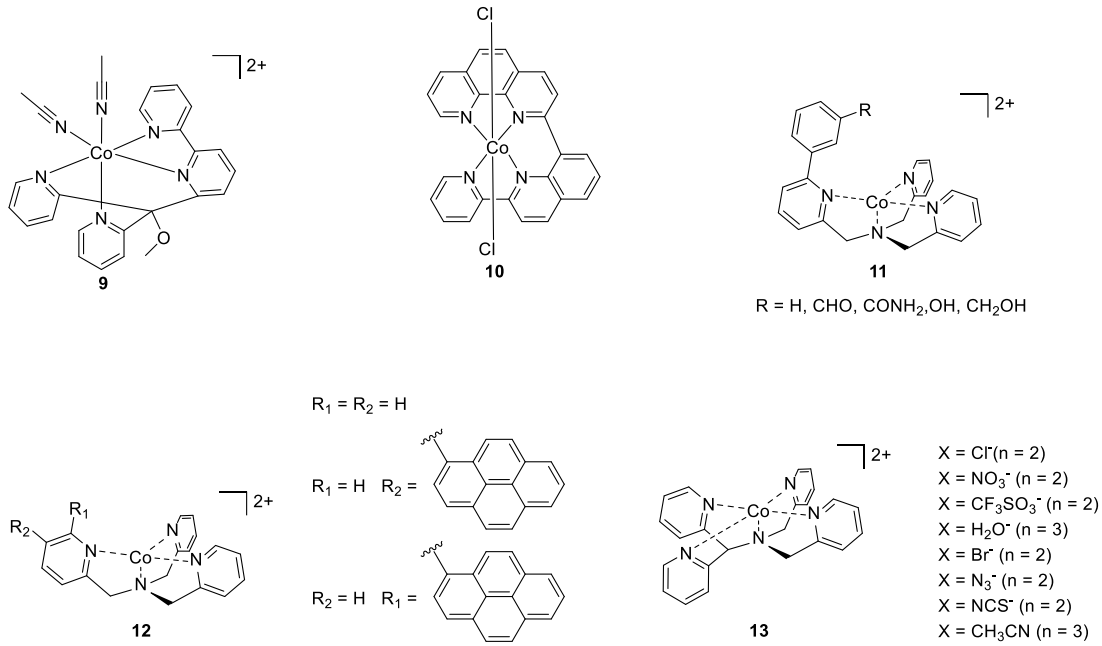

Figure 4: Cobalt complexes based on polypyridine or amino-polypyridines ligands for HER.

In the group where the thesis work was carried out, in 2016 a new cobalt complex based on **TPMA** ligands (**11**), was developed to promote hydrogen production with a lower overpotential in aqueous solutions under photochemical condition. The presence of substituents with different hydrogen bond donor or acceptor abilities, in the second coordination sphere, stabilized the catalytic unit.

In 2021 the group where the thesis was carried out, proposed a new use of **TPMA** complexes **12** to produce hydrogen. Hybrid electrodes have been developed based on the combination of carbon nanotubes and new cobalt complexes based on **TPMA** functionalized with pyrenes to allow anchoring to the carbon nanotube. This system can work in neutral aqueous solution and are able to produce H_2 also under lighted assisted conditions[11].

1.5 Carbon Dioxide Reduction

A promising alternative to the use of hydrocarbon sources for petrochemical raw materials and chemicals is to obtain energy-dense compounds by converting CO_2 into methanol or ethanol, formate and CO through electrochemical methods in which the electricity used can be stored and reused for other purposes [25-27]. In this approach, catalysis is of fundamental importance to find a new way to reuse carbon dioxide both photo and electrochemically. As a matter of fact, many catalysts were developed in the last years, and transition metal complexes supported by nitrogen donor ligands

constitute an important class for this purpose[28-31]. For these complexes, where the chelating ligand is highly basic, the Co(I) species are nucleophilic enough to coordinate the CO_2 molecule. This is experimentally proved by measuring the anodic shift of the half-wave ($E_{1/2}$) of the reduce couple Co_{II}/Co_I measured first under nitrogen and then under CO_2[33-35].

There are several mechanism hypotheses for the reduction of CO_2 to CO catalyzed by cobalt complexes.

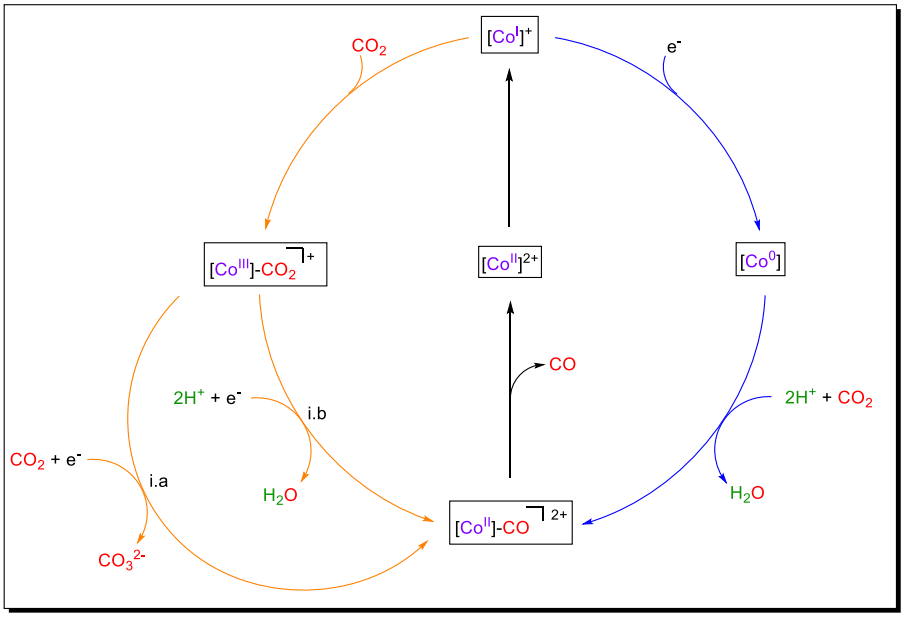

Scheme 3: Two proposed mechanisms from electrocatalytic reduction of CO_2 to CO catalysed by cobalt complexes based on nitrogen donor ligands. Orange route is proposed for cobalt catalyst with nitrogen donor ligand while blue route is for catalyst with less basic nitrogen donor ligands[48]

In the first route (**Scheme 3**, orange arrows) the critical steps for reducing CO_2 to CO (both electrochemically and photochemically) are the followings: i) the formation of adduct Co^{III}-CO_2 formed by the coordination of carbon dioxide with the Co^I species created *in situ* and ii) the breakdown of the C-O bond which can be promoted by another CO_2 molecule by releasing a CO_3^{2-} anion or by two hydrogen ions with the releasing of water molecule. In the second route, the formation of a Co^0 species is necessary to bind the CO_2 and reduce it (**Scheme 3**, blue arrows)[36].

Once reduced CO_2 to CO, the release of CO from the Co^{II}-CO adduct is usually quick, also because it is very rare to see this intermediate directly during an electrochemical analysis.

1.5.1 Cobalt TPMA complex for electrochemical reduction of CO_2

Cobalt and **TPMA** complex-based catalysts show good stability and TON potentials due to the strong chelating effect of the ligand. By acting on the applied potential and on the substituents of the pyridine rings in para position to minimize the perturbation of the steric properties of the compounds around the cobalt atom it is possible to increase the selectivity towards one of the two products (H_2 or CO) inhibiting the other. The electrochemical behaviour of these complexes was first tested under argon in DMF to see how it changes the reduction potential of the Co^{II}/Co^{I} species directly involved in coordinating CO_2.

In 2015 Cheng *et al* reported a robust cobalt catalyst for carbon dioxide reduction based on **TPMA** ligands complexed with cobalt chloride **20**. The isolated complex had a trigonal bipyramidal geometry confirmed by X-ray crystallographic analysis (**Figure 5a**). The reduction potential of Co^{II}/Co^{I} results more negative compared with other cobalt complexes supported by similar ligand scaffolds, and this may be crucial for an effective carbon dioxide reduction. For a reasonable bond of CO_2 with metal complexes the peak of $Co^{II/I}$ reduction should be more negative than 1,65 V.

The electrocatalytic current at the $Co^{II/I}$ reduction potential observed in the CO_2 atmosphere shows a marked increase indicating that the complex can be a good catalyst for reduction (**Figure 5b**).

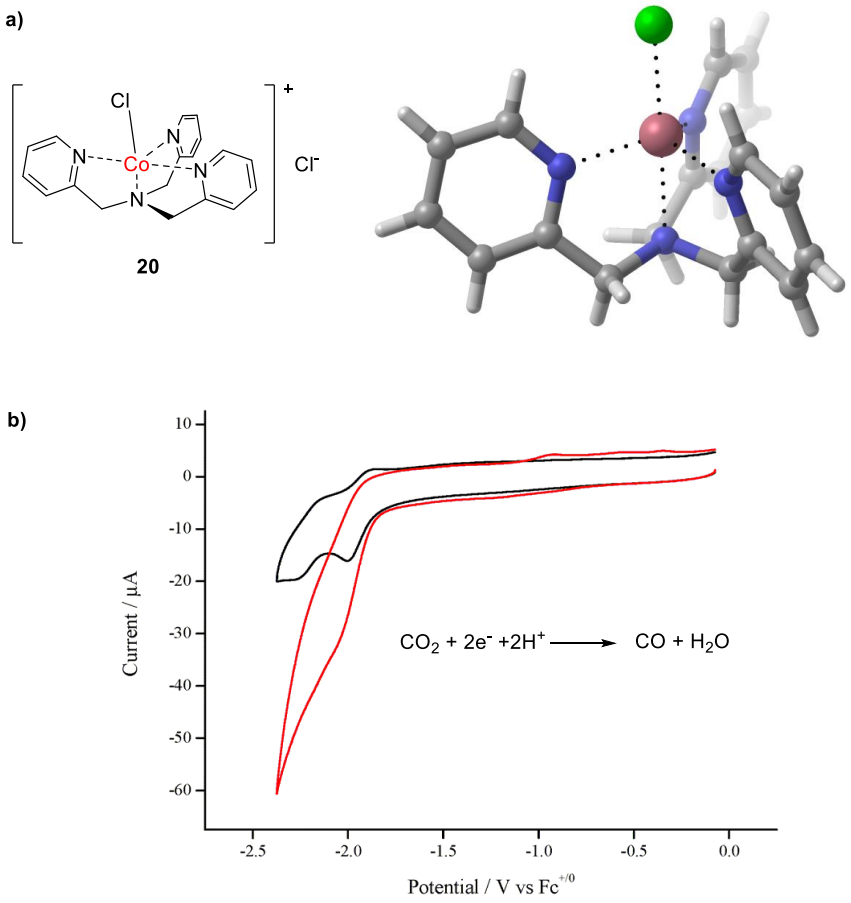

Figure 5: a) Cobalt **TPMA** complex structure and X-ray crystal. **b)** Cyclic voltammetry of Cheng's cobalt TPMA complex under argon (black) and carbon dioxide (red)[21] using a glassy carbon disk electrode, scan rate = 100 mV s^{-1}.

Another cobalt catalyst based on **TPMA** is reported by Zhu and others in 2016. In this case the skeleton of the **TPMA** is the same reported by Cheng (**20**) but the cobalt salt used is changed to evaluate the effect of the coordinate anion to cobalt. In particular, four cobalt salts were used and as a result four TPMA cobalt complexes, $[Co(TPMA)X]^+$ were studied where X = Cl^-, Br^-, I^-, NCS^- (**Figure 6**). The reduction peak of $Co^{II/I}$ is more negative with Cl^- as coordinated anion and with other this wave decreases in potential to -1.76 V. also in this case the adduct $[Co^I\text{-}CO_2]$ is form at first reduction peak of cobalt.

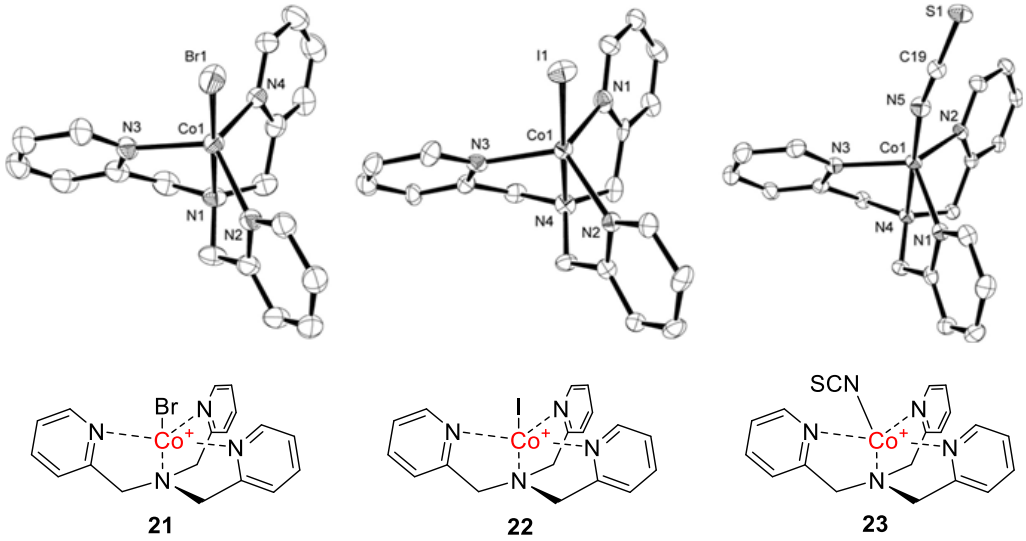

Figure 6: Structure of cobalt **TPMA** complex with different anion coordinated to cobalt: X = Br (**21**), I (**22**), NCS (**23**)[20].Counterions and solvents molecules have been removed for clarity.

The bromide ion demonstrates the best performance with TON >1000 and selectivity for CO >90%.

2. THE AIM OF THE THESIS WORK

This thesis focuses on the synthesis and characterization of new *para*-substituted TPMA-based cobalt complexes and some preliminary studies of their electrochemistry and their applications in reductive catalysis. When substituted, pyridine ligands show different electronic properties which are strictly connected with the nature of the substituents: as a matter of fact, pyridines carrying electron-withdrawing substituents show a more positive reduction potential while with electron-donating substituents more negative reduction potentials.

Specifically, the aim of this work is the synthesis and characterization of a chloro-substituted TPMA (for which chlorine is an electron-donating substituent) and the complexation with a cobalt salt in order to obtain **Co-TPMA** complexes. These complexes are then used for electrochemical reduction of CO_2 (**figure 7**), as discussed in **paragraph 1.5.1**.

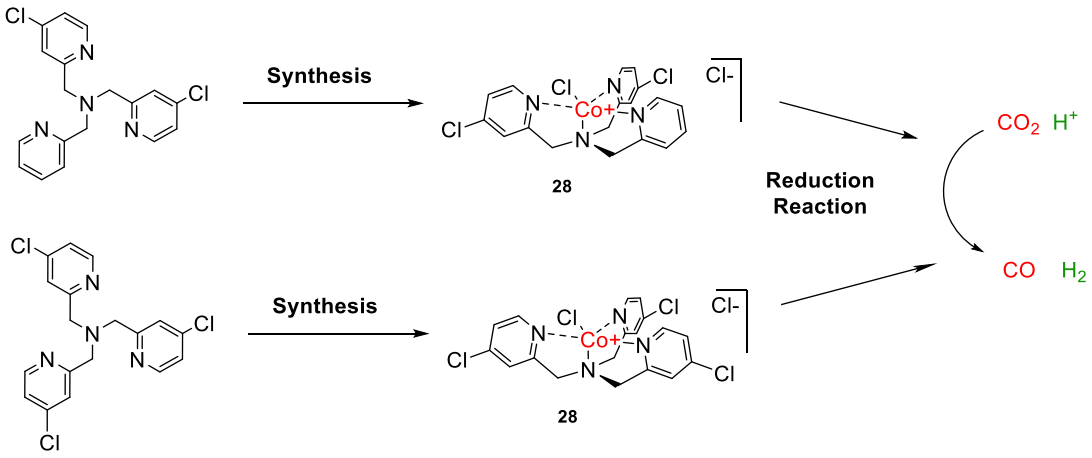

Figure 7: Schematic representation of the aim of the thesis work.

3. RESULTS AND DISCUSSION

3.1 Synthesis of *para*-substituted tris(2-pyridylmehyl)amine

This work targets the synthesis of *para*-substituted **TPMA** ligands with two or three substituents. Specifically, chlorine substituent has been chosen so its electron-withdrawing characteristics have been investigated.

While the direct introduction of a substituents position starting from a formed **TPMA** is difficult to achieve selectively, it is possible to obtain these types of products with a different design. The retrosynthetic approach is reported in **Scheme 4** and it shows the synthetic strategy used for the synthesis of ligands through the reductive amination reaction starting from the respective substituted aldehyde and a source of nitrogen which are pyridin-2-ylmethanamine for di-substituted and ammonium acetate for tri-substituted TPMA (**Scheme 4**). The reaction requires anhydrous conditions, under nitrogen and with dry DCM as the solvent using a mild reducing agent such as sodium triacetoxyborohydride.

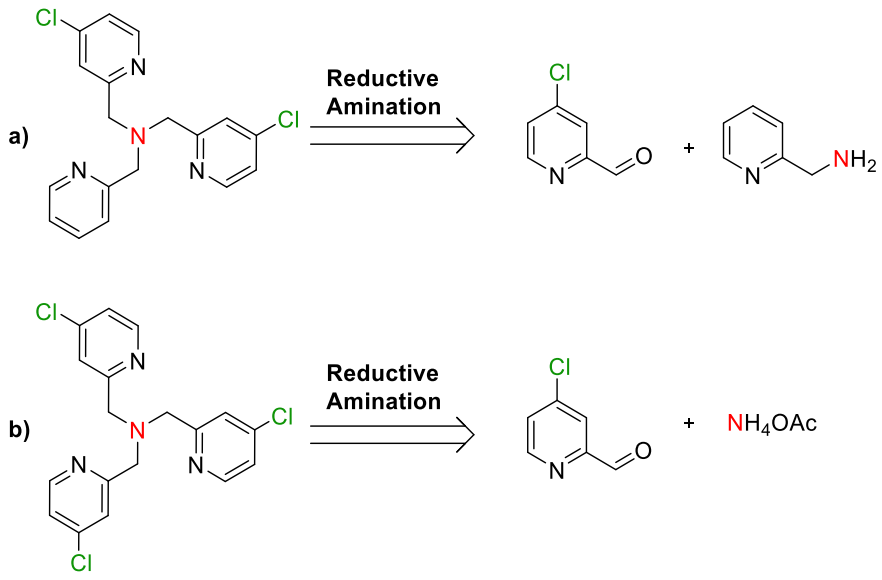

Scheme 4: Retrosynthetic approach adopted for the synthesis of **TPMA** with **a)** two and **b)** three chlorine substituents.

3.2 Chloro-substituted TPMA

The synthesis of **TPMA** with two and three chlorines as substituents follow the same reaction path. (**Scheme 5**).

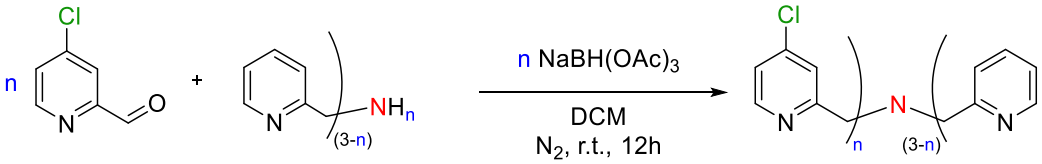

	Yield (%)	Name
n = 2	83	**Cl_2-TPMA 26**
n = 3*	32	**Cl_3-TPMA 27**

Scheme 5: Synthesis of **TPMA** ligands with chlorine as substituent through reductive amination reaction. *In the synthesis of **$(Cl)_3$-TPMA 27** the nitrogen source is ammonium acetate (NH_4OAc).

Firstly, 4-chloropicolinaldehyde and pyridin-2-ylmethanamine was dissolved in dry DCM under N_2 (to keep the reaction ambient dry) and left under stirring for 1 hour. Three aliquots of $NaBH(OAc)_3$ were added waiting 20 minutes between each other . The reactions were repeated once with the same amount of aldehyde and $NaBH(OAc)_3$. After that the reaction was stirred for 12 hours at room temperature. The solvent was removed under reduced pressure. The resulting solid was dissolved in EtOAc.

In general, after a simple work-up (which involves three extractions with KOH 0.1 M and a solution of brine to create a neater separation between the two phases), it is necessary to purify the ligand with a chromatographic column in both cases. The same eluent (gradient DCM:MeOH from 100:0 to 9:1), was used but different stationary phases were required: *di*-substituted **Cl_2-TPMA** in alumina gel to give a yellow oil in a good yield, whereas *tri*-substituted **Cl_3-TPMA** with silica gel to give an orange solid in low yield. That specific eluent gradient was used to avoid the protonation of the pyridine rings and the consequent broadening on the spot of the TLC. The gradual increase in the amount of methanol allows to selectively remove impurities and obtain the pure TPMA at the end of the column.

The yield for the synthesis of **27** is lower than that for **26** because part of the product was used to find the right eluent for the purification process.

3.3 Synthesis of Cobalt-TPMA complexes

The general procedure for the complexation of the Co (II) to the TPMA ligand was already reported in the literature and an adapted procedure was developed for this thesis work (**Scheme 6).**

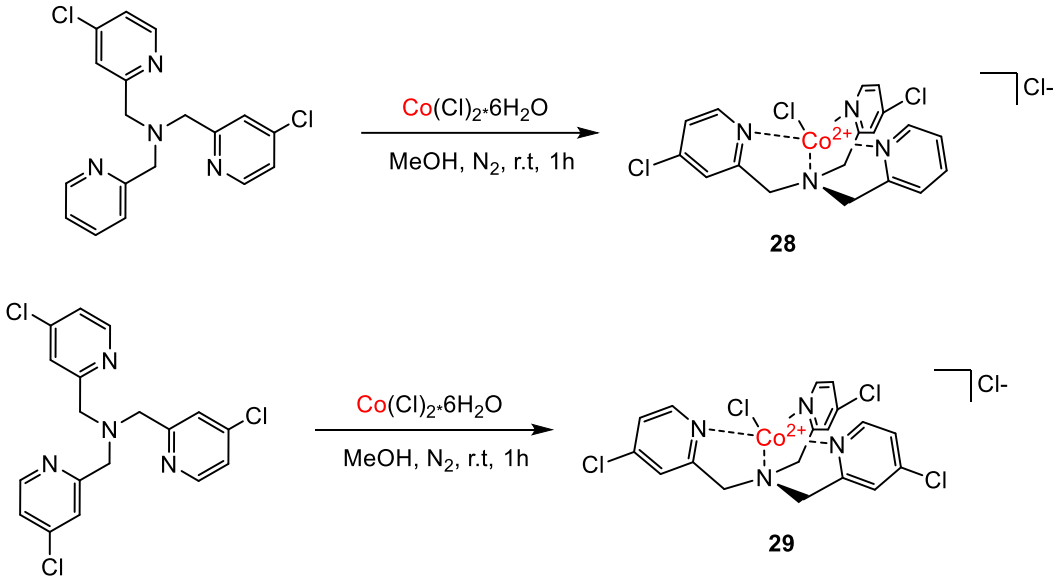

Name	Yield (%)
Co-Cl_2-TPMA	49
Co-Cl_3-TPMA	26

Scheme 6: Synthesis of cobalt-TPMA complexes using cobalt chloride hexahydride in MeOH under nitrogen atmosphere.

The TPMA ligand is dissolved in anhydrous methanol under stirring for a few minutes, keeping the environment under nitrogen. At this point, $CoCl_2$•$6H_2O$ is added and the reaction is left under stirring for two hours. At the end the MeOH is removed under reduced pressure and the solid is dissolved in the minimum amount of ACN. Precipitation is carried out by adding Et_2O and left under stirring for a few minutes, before separating it by centrifugation. At the end Et_2O is removed and the solid is dried under reduced pressure in a high vacuum pump for 3 hours. After the complexation, several crystallization attempts were performed to obtain crystals suitable for X-rays investigation. For this purpose, the vapor diffusion technique was used dissolving the complex in a small amount of acetonitrile and using the diethyl ether as the non-solvent that slowly diffuse into the complex solution. This translates in the use of a small aliquot of the solid which was dissolved in acetonitrile in a vial which in turn is inserted into a larger vial containing diethyl ether.

Complex **28** resulted in a purple solid whereas **29** in a green solid.

3.4 Cyclic Voltammetry

The synthetized cobalt complexes were also characterized though cyclic voltammetry (CV) to investigate the substituents effect on the Co^{II}/Co^{I} and Co^{I}/Co^{0} reduction potential. As reported in the introduction part (**paragraph 3.3**), the typical CV plot of a TPMA cobalt (II) complex shows two characteristic irreversible reduction peaks centred at -1,54 V and -1,76 V vs Ag/AgCl which are assigned as Co^{II}/Co^{I} and Co^{I}/Co^{0} reduction respectively. The introduction of a para substituent on the TPMA skeleton have a crucial impact on the electrochemical properties of the metal complex also influencing the reduction peaks of the cobalt. **Figure 11** shows the CV plots for the *di* and *tris* substituted complexes and as expected, the two reduction waves of the metal center are influenced by the presence of the substituents. In particular, the electron-withdrawing and electron-donating nature of the substituent is associated with a positive and negative shift of the reduction potential respectively: in the case of chlorine substituents, the peak is shifted towards more positive potentials.

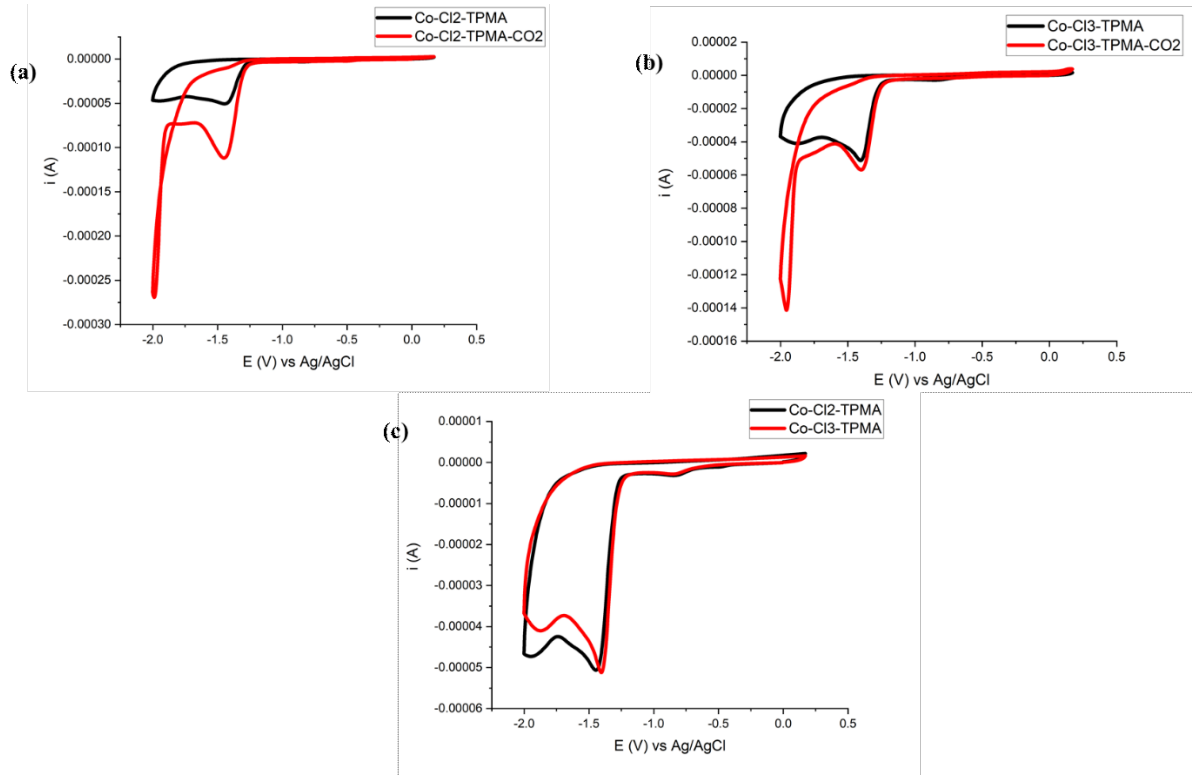

Figure 11: a) CV of **28** under N_2 (black) CO_2 (red); **b)** CV of **29** under N_2 (black) CO_2 (red); **c)** Superimposition CV under N_2 of **28** (black) and **29** (red).

The reduction peaks are irreversible for both complexes. Complex **28** shows its reduction peaks with E_{pc} at E=1.70 V and E= 1.49 V, whereas complex **29** at E=1.67 V and E=1.47 V. The electron-withdrawing effect is confirmed and analysing the superimposition CV it appears evident how adding the third chloro-group to the rings (**29**) causes the peaks to shift a little more towards positive potentials in comparison with the *di*-substituted complex **28.**

4 CONCLUSIONS

In this thesis, a TPMA-based ligand with two chloro-groups was synthetized and characterized, as well as the relative Cobalt (II) complex. In addition, a Cobalt (II) complex with a TPMA-based ligand having three chlorine was synthetized and its properties were compared to the former complex.
A general methodology for the purification of ligands has been used and it consists in the use of a chromatographic column using a gradient eluent DCM:MeOH (from DCM to DCM:MeOH 9:1).

The two complexes revealed to be stable solids once precipitated and dried under vacuum and one of their most noticeable characteristics was their colors: *di*-chloro ligand appeared to be purple whereas *tri*-chloro became a green solid.

The identity of the ligands was confirmed analysing the ^{1}H-NMR spectra. Both a 300 Hz and a 400 Hz instruments were used, and it is evident how increasing the frequency results in more wide and definite peaks.

The electrochemical analysis carried out on the complexes was influenced by the nature of the substituents in *para*-position: by inserting and electron-withdrawing substituent, the reduction potential shifted towards more positive potentials.

The latter work mainly refers to applications of TPMA-based ligands in reductive catalysis of CO_2 and H_2, but there are other several fields such as sensing technologies in which those ligands could be applied.

5 EXPERIMENTAL PART

5.3 General methods

NMR spectra were recorded at 301 K on Bruker Avance DMX 400 MHz and Bruker Avance 300 MHz instruments. All the ^{1}H-NMR spectra were referenced to residual isotopic impurity of $CDCl_3$ (7.26 ppm) or CD_3CN (1.94 ppm). The following abbreviations are used in reporting the multiplicity for NMR resonances: s=single, d=doublet, t= triplet, q=quartet, and m=multiplet. The NMR data were processed using MestReNova 12.0.2.

Cyclic voltammetries were recorded with AUTOLAB PGSTAT101 managed by PC with NOVA 2.1 software interface. All the experiment were conducted using a three-electrode system consisting of a working electrode (WE, *glassy carbon electrode* ϕ = 3 mm, Basi), reference electrode (RE, *Ag/AgCl, 3M NaCl*) and counter electrode (CE, *platinum electrode* ϕ = 1.6 mm, Basi).

Chemicals were purchased from Aldrich or FluoroChem and used without further purification.

5.4 Abbreviations

ACN Acetonitrile

DCM Dicloromethane

EtOAc Etil acetate

Et_2O Diethyl Ether

MeOH Methanol

TPMA Tris((pyridin-2-yl)methyl)amine

5.5 Characterization of 1-(4-chloropyridin-2-yl)-N-((4-chloropyridin-2-yl) methyl-N-(pyridine-2-ylmethyl)methanamine 26

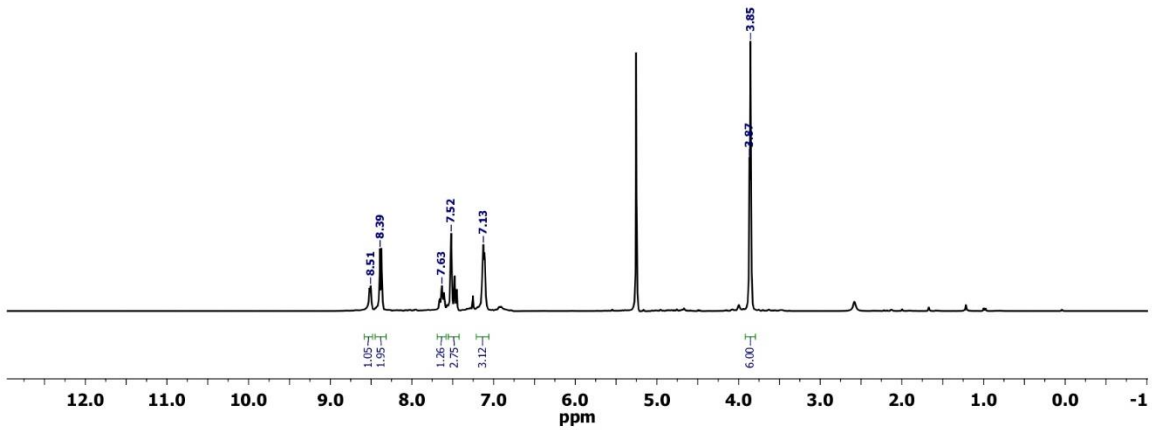

Figure 8: ^{1}H-NMR (300 MHz, $CDCl_3$) of 1-(4-chloropyridin-2-yl)-N-((4-chloropyridin-2-yl) methyl-N-(pyridine-2-ylmethyl)methanamine

The ligand **26** was characterized with ^{1}H-NMR, which confirmed its identity. ^{1}H-NMR spectrum revealed a singlet referred to the six benzylic protons at 3.86 ppm, then signals for the pyridine protons can be detected (7.12 ppm, 7.47 ppm, 7.62 ppm, 8.38 ppm and 8.51 ppm). The most recognisable signals are those at 8.38 ppm and 8.51 ppm which stand for the alpha protons of the pyridine rings; it is clear how the pyridyl nitrogen has a higher electron-withdrawing effect compared with chlorine substituent, so the alpha proton on the pyridyl ring that has no chlorine atoms appears to be more deshielded. In this spectrum, a slightly high signal at 5.25 ppm can be noticed: this could be due to traces of methanol used as eluent in the purification process, as discussed in **paragraph 3.2**.

5.6 Characterization of Co-TPMA complexes 28-29

The main difference between these spectra and the one for the TPMA-ligand is that the characteristic peaks of the cobalt complexes reach 130 ppm (**figure 9-10**), whereas ligand's signals fall between -1 and 12 ppm (as reported in **figure 8**). This is caused by the fact that Co^{2+}, as many transition metal ions, has a large magnetic susceptibility anisotropy: its presence causes line broadening of all NMR signals from nuclei close to the metal ion.

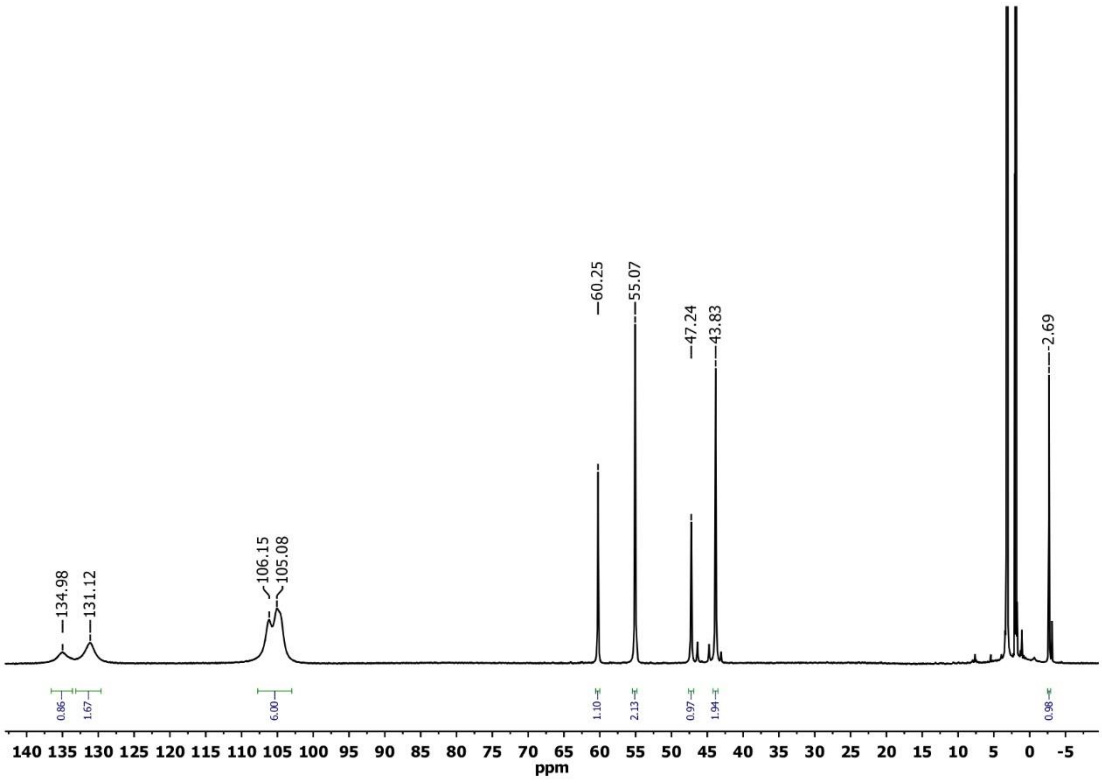

Figure 9: Characterization of Co-Cl_2-TPMA **28**

The spectrum revealed all the main peaks: alpha pyridyl protons fall at 134.98 ppm and 131.12 ppm, while benzyl protons fall at 106.15 ppm and 105.08 ppm. Between 60 and 40 ppm the aromatic protons on pyridine rings can be found: those are all singlets that refer to protons in *meta*-position and the most shielded ones are those situated in the unsubstituted pyridine ring. At -2.69 ppm the singlet for the proton in *para*-position can be found.

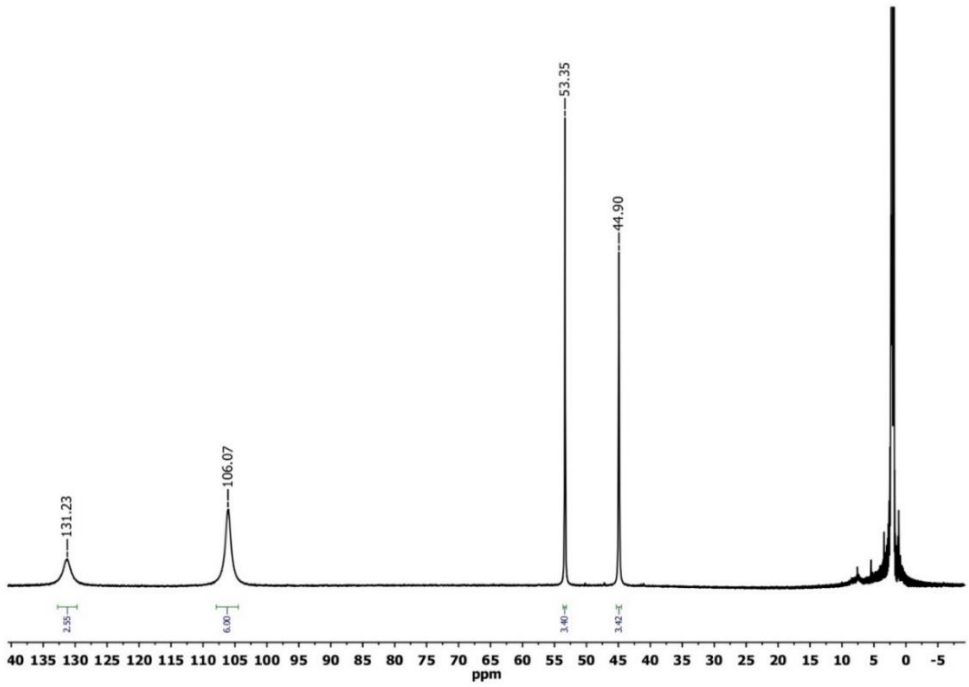

Figure 10: Characterization of Co-Cl_3-TPMA **29**

For Co-Cl_3-TPMA the main peaks can be detected: alpha pyridyl protons fall at 131.23 ppm and benzyl protons fall at 106.07 ppm. Other recognisable signals are those between 50 and 40 ppm that stand for aromatic protons on the pyridine rings: two singlets that stand for three protons each, so it's a different situation compared with **28**. The singlet at 55.35 ppm is for the protons in *meta*-positions that are closer to the central nitrogen atom, whilst the one at 44.90 ppm represents the other protons in *meta*-positions. It is evident that this is a *para*-substituted ligand with three identical substituents because all three para-positions are occupied by chlorine substituents and no signal between -1 and 0 ppm can be revealed.

6 REFERENCES

(1) T. P. Yoon, E. N. Jacobsen, *Science* **2003**, *299*, 1691.

(2) Leenders, S. H. A. M.; Gramage-Doria, R.; de Bruin, B.; Reek, J. N. H. *Chem. Soc. Rev*. **2015**, 433-448.

(3) Bravin, C.; Badetti, E.; Licini, G.; Zonta, C., *Coord. Chem. Rev*., **2021**, *427*, 213558.

(4) Blackman, A. G., *Eur. J. Inorg. Chem*. **2008**, 2633

(5) Anderegg, G.; Wenk, F., *Helv. Chim. Acta* **1967**, *50*, 2330–2332.

(6) Anderegg, G.; Hubmann, E.; Podder, N. G.; Wenk, F., *Helv. Chim. Acta* **1977**, *60*, 123–140.

(7) da Mota, M. M.; Rodgers, J.; Nelson, S. M., J. *Chem. Soc. A* **1969**, 2036–2044.

(8) Szajna, E.; Dobrowolski, P.; Fuller, A. L.; Arif, A. M.; Berreau, L. M., *Inorg. Chem*. **2004**, *43*, 3988–3997

(9) Alain, D.; Hagen, K. S., *Inorg. Chem*., **1998**, *37*, 215-223

(10) Natali, M.; Badetti, E.; Deponti, E.; Gamberoni, M.; Scaramuzzo, F. A.; Sartorel, A.; Zonta, C., *Dalton Transactions* **2016**, *45*, 14764–14773

(11) Benazzi, E.; Begato, F.; Niorettini, A.; Destro, L.; Wurst, K.; Licini, G.; Agnoli, S.; Zonta, C.; Natali, M., *J. Mater. Chem*. *A* **2021**, *9*, 20032–20039.

(12) Carmo dos Santos, N. A.; Lorandi, F.; Badetti, E.; Wurst, K.; Isse, A. A.; Gennaro, A.; Licini, G.; Zonta, C., *Polymer* **2017**, *128*, 169–176.

(13) Chan, S. L. F.; Lam, T. L.; Yang, C.; Lai, J.; Cao, B.; Zhou, Z.; Zhu, Q., *Polyhedron* **2017**, *125*, 156–163.

(14) Chan, S. L. F.; Lam, T. L.; Yang, C.; Yan, S. C.; Cheng, N. M., *Chem. Comm.* **2015**, *51*, 7799–7801

(15) Joyce, L. A.; Maynor, M. S.; Dragna, J. M.; da Cruz, G. M.; Lynch, V. M.; Canary, J. W.; Anslyn, E. V., J. *Am. Chem. Soc*. **2011**, *133*, 13746–13752

(16) You, L.; Pescitelli, G.; Anslyn, E. v.; di Bari, L., J. *Am. Chem. Soc*. **2012**, *134*, 7117–7125

(17) Energy Agency, I. *Review 2021 Assessing the Effects of Economic Recoveries on Global Energy Demand and CO 2 Emissions in 2021 Global Energy*; **2021**

(18) Pellegrin, Y.; Odobel, F., *C. R. Chimie*. **2017**, *20*, 283

(19) Deponti, E.; Luisa, A.; Natali, M.; Iengo, E.; Scandola, F., *Dalton Trans*. **2014**, *43*, 16345–16353.

(20) Krishnan, C. V.; Sutin, N., J. *Am. Chem. Soc*. **1981**, *103*, 2141-2142

(21) Krishnan, C. V.; Brunschwig, B. S.; Creutz, C.; Sutin, N., *J. Am. Chem. Soc.* **1985**, *107*, 2005-2015.

(22) Bigi, J. P.; Hanna, T. E.; Harman, W. H.; Chang, A.; Chang, C. J., *Chem. Comm*. **2010**, *46*, 958–960.

(23) Tong, L.; Zong, R.; Thummel, R. P., J. *Am. Chem. Soc*. **2014**, *136*, 4881–4884.

(24) Lo, W. K. C.; Castillo, C. E.; Gueret, R.; Fortage, J.; Rebarz, M.; Sliwa, M.; Thomas, F.; McAdam, C. J.; Jameson, G. B.; McMorran, D. A.; Crowley, J. D.; Collomb, M. N.; Blackman, A. G., *Inorg. Chem*. **2016**, *55*, 4564–4581

(25) Wang, W. H.; Himeda, Y.; Muckerman, J. T.; Manbeck, G. F.; Fujita, E., *Chem.*

Rev. **2015**, 12936–12973.
(26) Reda, T.; Plugge, C. M.; Abram, N. J.; Hirst, J., *PNAS* **2008**, *105*, 10654-10658.
(27) Qiao, J.; Liu, Y.; Hong, F.; Zhang, J., *Chem. Soc. Rev*. **2014**, 631–675.
(28) Lacy, D. C.; McCrory, C. C. L.; Peters, J. C., *Inorg. Chem*. **2014**, *53*, 4980–4988.
(29) Elgrishi, N.; Chambers, M. B.; Fontecave, M., *Chem. Sci*. **2015**, *6*, 2522–2531.
(30) Cometto, C.; Chen, L.; Lo, P. K.; Guo, Z.; Lau, K. C.; Anxolabéhère-Mallart, E.; Fave, C.; Lau, T. C.; Robert, M., *ACS Catal*. **2018**, *8*, 3411–3417.
(31) Shimoda, T.; Morishima, T.; Kodama, K.; Hirose, T.; Polyansky, D. E.; Manbeck, G. F.; Muckerman, J. T.; Fujita, E., *Inorg. Chem*. **2018**, *57*, 5486–5498.
(32) Wang, J. W.; Huang, H. H.; Sun, J. K.; Ouyang, T.; Zhong, D. C.; Lu, T. B., *ChemSusChem* **2018**, *11*, 1025–1031.
(33) Gangi, D. A.; Durand, R. R., J. *Am. Chem. Soc*. **1986**.
(34) Koster; Thewissen; Mackor; Beley; Collin; J-p; Sauvage; Petit; Chartier., *J. Am. Chem. Soc.* **1990**, *112*, 3420-3426.
(35) Schneider, J.; Jia, H.; Muckerman, J. T.; Fujita, E., *Chem. Soc. Rev.* **2012**, *41*, 2036–2051.
(36) Fernández, S.; Franco, F.; Casadevall, C.; Martin-Diaconescu, V.; Luis, J. M.; Lloret-Fillol, J., J *Am Chem Soc*. **2020**, *142*, 120–133.